In vitro evaluation of protein–protein interactions in the rice KAI2 ligand signaling complex

Keita Tanaka[1,2], Jiawang Wu[1,2], Qianwei Xia[3,4], Yutaro Harada[5], Taiki Suzuki[5], Yujiao Yan[1,2], Yoshiya Seto[5], Guosheng Xiong[3,4], Hiromu Kameoka[1,2,*]

1. Key Laboratory of Plant Carbon Capture, CAS Centre for Excellence in Molecular Plant Sciences, Chinese Academy of Sciences, 300 Fenglin Road, Shanghai 200032, China.
2. CAS-JIC Centre of Excellence for Plant and Microbial Science (CEPAMS), Center for Excellence in Molecular Plant Sciences, Chinese Academy of Sciences, 300 Fenglin Road, Shanghai 200032, China.
3. State Key Laboratory of Crop Genetics & Germplasm Enhancement and Utilization, College of Life Sciences, Nanjing Agricultural University, Nanjing, 210095, China
4. Plant Phenomics Research Center, Academy for Advanced Interdisciplinary Studies, Nanjing Agricultural University, Nanjing, 210095, China
5. Laboratory of Plant Chemical Regulation, School of Agriculture, Meiji University, 1-1-1 Higashi-Mita, Tama-ku, Kawasaki, Kanagawa 214-8571, Japan.

*: corresponding author

Contact: khiromu@cemps.ac.cn

The author responsible for distribution of materials integral to the findings presented in this article in accordance with the policy described in the Instructions for Authors (https://academic.oup.com/plphys/pages/General-Instructions) is Hiromu Kameoka.

Running head: Protein–protein interactions in the rice KL signaling complex

Abstract

KARRIKIN INSENSITIVE 2 (KAI2)/DWARF14-LIKE (D14L) plays key roles in land plant development, environmental responses, and the establishment of arbuscular mycorrhizal symbiosis, likely acting as the receptor for unidentified signaling molecules termed KAI2 ligands (KLs). KL perception by KAI2/D14L promotes DWARF3 (D3)/MORE AXILLARY GROWTH2 (MAX2) F-box protein-mediated ubiquitination of SUPPRESSOR OF MAX2 1 (SMAX1) proteins, thereby transducing the KL signals. Although genetic and *in vivo* assays have demonstrated the functions of these components, the biochemical details of their interactions remain elusive. Here we investigated physical interactions between rice D14L, D3, and OsSMAX1 *in vitro* using desmethyl germinone (dMGer), a recently developed KL analog. dMGer elicited KL responses in rice with higher activity and pathway specificity than a widely used KL analog (−)-GR24. dMGer, but not (−)-GR24, directly bound to D14L and promoted the interaction between D14L and D3 *in vitro*. The interaction between D14L and OsSMAX1 was also enhanced by dMGer. Furthermore, we identified the domain of OsSMAX1 that distinguishes it from its paralog DWARF53 (D53), which is associated with the strigolactone signaling complex. These findings propose a model of the interactions among KL signaling components and highlight the role of the ligand in the signaling complex.

Keywords: KARRIKIN INSENSITIVE2 (KAI2)/DWARF14-LIKE (D14L), DWARF3 (D3)/MORE AXYLLARY GROWTH2 (MAX2), SUPPRESSOR OF MAX2 1 (SMAX1), KAI2 ligand (KL), desmethyl germinone (dMGer), protein–protein interaction

Introduction

The α/β-fold hydrolase KARRIKIN INSENSITIVE2 (KAI2)/DWARF14-Like (D14L) is conserved in land plants and regulates diverse aspects of their life cycles. *KAI2* was first identified in *Arabidopsis thaliana* (Arabidopsis) as a gene essential for the response to karrikins (KARs), a group of smoke-derived butenolides that stimulate seed germination and photomorphogenesis (Chiwocha et al., 2009; Waters et al., 2012). *KAI2*/*D14L* regulates not only seed germination and photomorphogenesis but also root development (Villaécija-Aguilar et al., 2019; Carbonnel et al., 2020; Meng et al., 2022), drought response (Li et al., 2017), arbuscular mycorrhizal (AM) symbiosis (Gutjahr et al., 2015), etc. Notably, KARs are absent in living plants, whereas *kai2*/*d14l* mutants exhibit phenotypes opposite to those induced by KAR treatment in wild-type (WT) plants. For example, KAR treatment suppresses mesocotyl elongation in *Oryza sativa* (rice) in the dark, whereas *d14l* mutants exhibit elongated mesocotyls (Gutjahr et al., 2015; Zheng et al., 2020). These findings suggest that KAI2/D14L mediates responses to an unidentified endogenous compound distinct from KARs. Since KAI2/D14L is considered to be its receptor, this putative compound is referred to as KAI2 ligand (KL) (Conn and Nelson, 2016).

The KL signaling pathway is composed of components of the strigolactone (SL) signaling pathway or their paralogs. In SL signaling, SLs bind to DWARF14 (D14)/DECREASED APICAL DOMINANCE2/RAMOSUS3, a paralog of KAI2/D14L, promoting the interaction of D14 with the F-box protein MORE AXILLARY GROWTH2 (MAX2)/DWARF3 (D3) in an Skp, Cullin, F-box (SCF) complex. D14 also interacts with the repressor of the SL signal, DWARF53 (D53) in rice or SUPPRESSOR OF MAX2 1 (SMAX1)-LIKE6/7/8 (SMXL6/7/8) in Arabidopsis, in an SL-dependent manner (Jiang et al., 2013; Zhou et al., 2013; Wang et al., 2015; Wang et al., 2020a; Soundappan et al., 2015). SLs thus trigger the formation of a D14-$SCF^{MAX2/D3}$-D53/SMXL6/7/8 complex and subsequent ubiquitination and 26S-proteasomal degradation of the repressor D53/SMXL6/7/8 proteins, thereby inducing SL responses. On the other hand, in KL signaling, KL is considered to be perceived by KAI2/D14L, which triggers the formation of the KAI2/D14L–$SCF^{MAX2/D3}$–SMAX1/SMXL2/OsSMAX1 complex and their degradation. However, the protein–protein interactions among the KL signaling components have been less well characterized than those in the SL signaling components.

Evidence for the ligand-dependent interactions among the KL signaling components remains limited. In Arabidopsis, although an *in vitro* pull-down assay shows that KAI2 and

84 MAX2 slightly interact in a ligand-dependent manner, this interaction is much weaker than that
85 that observed between AtD14 and MAX2 detected under the same conditions (Xu et al., 2018).
86 Ligand-dependent interaction between KAI2 and SMAX1 has been demonstrated only by *in*
87 *vivo* co-immunoprecipitation or yeast two-hybrid assays, but not by *in vitro* pull-down assays
88 (Khosla et al., 2020; Yao et al., 2021; Okabe et al., 2023). In rice, ligand-dependent interactions
89 among the KL signaling components have not been reported. Overall, the available evidence is
90 insufficient to determine whether the ligands induce direct interactions among the KL signaling
91 components.

92 The functions of the domains of the KL signaling components are also poorly understood.
93 SMXL proteins contain conserved domains, N-terminal domain (N), putative ATPase domain
94 1 (D1), middle region (M), and C-terminal putative ATPase domain 2 (D2). The D2 domain is
95 required for MAX2/D3-mediated degradation (Jiang et al., 2013; Zhou et al., 2013; Wang et
96 al., 2020b; Khosla et al., 2020). Yeast two-hybrid assays have shown that the D1, or D1 and M
97 (D1M) domains are responsible for the ligand-dependent interaction with D14 or KAI2/D14L
98 (Zhou et al., 2013; Khosla et al., 2020). In contrast, another study reported that the D53-D2
99 domain alone interacts with D14 and that this interaction is enhanced by the C-terminal α-helix
100 of D3 (D3-CTH). Binding of D3-CTH suppresses the ligand-hydrolysis activity of D14
101 (Shabek et al., 2018). Expression of *MAX2* lacking CTH failed to fully rescue the *max2* mutant
102 phenotypes associated with both SL and KL. Furthermore, mutations in the CTH of D3 or
103 MAX2 showed altered their activity to regulate the hydrolase activity of KAI2 and the SMAX1
104 ubiquitination, suggesting the involvement of D3/MAX2-CTH in KL signaling (Tal et al.,
105 2022; Tal et al., 2023). However, the role of the CTH in the interactions among the KL signaling
106 components remains to be elucidated.

107 A possible reason for the limited evidence of the *in vitro* interaction is insufficient
108 activation of KAI2/D14L by KARs or artificial KL analogs. Differential scanning fluorimetry
109 (DSF) has been used to evaluate the activity of the putative ligands of D14 or KAI2/D14L, in
110 which the shifts in thermal stability (melting temperature; Tm) of the proteins indicate
111 structural changes induced by ligand binding (Niesen et al., 2007). Previous works suggest that
112 not ligand binding alone but the shift in receptor stability in DSF is the better indicator of ligand
113 activity (Seto et al., 2019; Kushihara et al., 2025). Natural SLs and (+)-GR24, an artificial SL
114 analog, induce large shifts towards destabilization of D14 (Hamiaux et al., 2012; Abe et al.,
115 2014; de Saint Germain et al., 2016; Seto et al., 2019; Yao et al., 2021) (Supplementary Figure
116 S1). On the other hand, KARs do not induce shifts in KAI2/D14L (Waters et al., 2015; Fukui

et al., 2019). This result has raised a hypothesis that the direct ligands of KAI2/D14L are not KARs themselves, but uncharacterized metabolite(s) derived from KARs in plants. Interestingly, (−)-GR24 (Supplementary Figure S1), a widely used artificial KL analog, induces only slight shifts in KAI2 stability in Arabidopsis (Fukui et al., 2019; Yao et al., 2021). Moreover, it does not induce shifts in some species, including rice, *Brachypodium distachyon*, and *Selaginella moellendorffii* (Waters et al., 2015; Yao et al., 2021; Meng et al., 2022). These results suggest the possibility that (−)-GR24 does not possess sufficient activity to enhance the interactions between the KL signaling components.

Recently, a new type of compounds, desmethyl butenolides, has been reported to function as KL analogs (Yao et al., 2021). While natural SLs, artificial SL analogs, and (−)-GR24 have a methyl group on their butenolide ring, desmethyl-type KL analogs lack this methyl group. Currently, four types of desmethyl-type KL analogs, desmethyl Yoshimulactone Green (dYLG, Supplementary Figure S1), desmethyl-GR24 (dGR24), desmethyl-CN-debranone, and desmethyl germinone (dMGer, Supplementary Figure S1), have been developed (Yao et al., 2018; Yao et al., 2021; Okabe et al., 2023). dYLG binds to the ligand binding pocket of KAI2/D14L and emits fluorescence upon hydrolysis by KAI2/D14L. The other three compounds have been shown to induce stronger KL responses *in vivo* and larger stability shifts of KAI2/D14L in DSF than (−)-GR24 (Yao et al., 2021; Meng et al., 2022; Okabe et al., 2023; Kushihara et al., 2025). dMGer reportedly induces the interaction between Arabidopsis KAI2 and SMAX1 in yeast two-hybrid assays (Okabe et al., 2023; Kushihara et al., 2025). However, the ability of desmethyl butenolide-type ligands to induce the *in vitro* interactions of the KL signaling components has not yet been examined.

Here, we investigate the rice KL signaling using artificial KL analogs, (−)-GR24 and dMGer to address key questions: whether these KL analogs directly bind to the receptor and elicit physiological responses across species; whether the KL signaling components directly interact and, if so, which interactions are mediated by KL; and which domain is pivotal for the interactions among the components. Pharmacological assays reveal that dMGer activates the KL signaling pathway more strongly and specifically than (−)-GR24 in rice. *In vitro* assays demonstrate that D14L recognizes dMGer, but not (−)-GR24. We then verified interactions among D14L, D3, and OsSMAX1, providing direct evidence for the enhancement of D14L–D3 and D14L–OsSMAX1 interactions *in vitro*. Furthermore, by assaying the interactions among D14L, D14, and domains of OsSMAX1 and D53, we reveal the functions of the

domains that underlie the specific interactions of D14L–OsSMAX1 and D14–D53. Thus, our study refines the biochemical understanding of the KL signaling pathway.

Results

dMGer induces KL responses in rice

While the activities of desmethyl-type KL analogs have been assessed with D14L/KAI2 from several species *in vitro*, their KAI2/D14L-dependent activities *in vivo* have been examined only in Arabidopsis. dMGer, a recently developed desmethyl-type KL analog, promotes seed germination and inhibits hypocotyl elongation in Arabidopsis in a KAI2-dependent manner (Okabe et al., 2023; Kushihara et al., 2025). To evaluate the activities of dMGer as a KL analog, we examined the responses of rice to dMGer.

We first assessed the dMGer activity on mesocotyl length. Elongation of mesocotyls in dark-grown rice seedlings is a well-characterized phenotype regulated by the KL signaling pathway (Kameoka and Kyozuka, 2015; Gutjahr et al., 2015; Choi et al., 2020; Zheng et al., 2020). *d14l* mutants exhibit longer mesocotyls than WT, whereas KARs and (−)-GR24 suppress mesocotyl elongation in a *D14L*-dependent manner (Zheng et al., 2020). We compared mesocotyl length of seedlings grown in the dark with or without 1 μM dMGer treatment. WT seedlings treated with dMGer developed shorter mesocotyls than those of the control group (Figure 1A and 1B). In contrast to WT seedlings, *d14l* seedlings showed no significant difference in mesocotyl length between dMGer-treated and untreated groups (Figure 1A and 1B). These results indicate that dMGer suppresses mesocotyl elongation through the KL signaling pathway in rice.

Next, we characterized the effects of dMGer on transcriptional responses of rice KL-responsive markers, *D14-LIKE2b* (*DLK2b*) (Os01g0595600) and *KARRIKIN-UP-REGULATED F-BOX1* (*KUF1*) (Os06g0711700), to dMGer treatment, comparing them with those induced by (−)-GR24. Previous studies have shown that, across land plant species, homologues of these genes are induced by the KL signals (Waters et al., 2012; Choi et al., 2020; Zheng et al., 2020; Mizuno et al., 2021; Sepulveda et al., 2022; Meng et al.). In WT seedlings, dMGer induced the expression of *DLK2b* (Figure 1C) and *KUF1* (Figure 1D) in a dose-dependent manner. Across all concentration tested, dMGer induced transcription of

179 *DLK2b* to a greater extent than (−)-GR24 (Figure 1C). A similar trend was observed for *KUF1*
180 in plants treated with 1 μM and 10 μM of these chemicals (Figure 1D). These results indicate
181 that dMGer induces stronger transcriptional activation of KL-responsive markers in rice than
182 (−)-GR24. To determine whether these responses require *D14L*, we examined the responses in
183 *d14l* mutant seedlings. In *d14l*, 10 μM dMGer did not induce either *DLK2b* (Figure 1E) or
184 *KUF1* (Figure 1F). In contrast, 10 μM (−)-GR24 strongly induced *DLK2b* (Figure 1E). The
185 expression of *KUF1* also tended to be induced by (−)-GR24 (Figure 1F). These results indicate
186 that dMGer induces the expression of these genes depending on *D14L*, whereas (−)-GR24 also
187 acts *D14L*-independently.

188 Furthermore, we examined the effect of dMGer on OsSMAX1 protein stability *in vivo*.
189 Treatment with 1 μM dMGer led to a marked reduction in OsSMAX1 levels in WT plants
190 within two hours. Consistent with the transcriptional analyses of the KL-responsive marker
191 genes, 1 μM (−)-GR24 also triggered a reduction in OsSMAX1 levels, albeit to a lesser extent
192 than dMGer. In *d14l* mutants, OsSMAX1 levels remained unaffected following treatment with
193 either 1 μM or 10 μM dMGer treatment, while OsSMAX1 levels were reduced by 10 μM (−)-
194 GR24 treatment (Figure 1G). These results suggest that dMGer promotes the degradation of
195 OsSMAX1 in a *D14L*-dependent manner. Together, these findings demonstrate that dMGer
196 functions as an effective and selective KL analog in rice *in vivo*.

197 **dMGer binds to D14L and induces its structural changes *in vitro***

198 We then examined whether dMGer directly interacts with D14L. We first conducted dYLG
199 (Supplementary Figure S1) assays. dYLG is hydrolyzed in the ligand-binding pocket of
200 D14L/KAI2 and releases a fluorophore. In this assay, the test compounds and dYLG are co-
201 incubated with recombinant D14L/KAI2. Test compounds that bind to the ligand-binding
202 pocket of D14L/KAI2 reduce the fluorescence of the dYLG-derived fluorophore by
203 competitively inhibiting the hydrolysis of dYLG. D14L was incubated with 1 μM dYLG and
204 different concentrations of dMGer or (−)-GR24. dMGer significantly reduced dYLG
205 hydrolysis at 1 μM and almost completely abolished it at 5–10 μM (Figure 2A). By contrast,
206 (−)-GR24 did not affect dYLG hydrolysis even at 10 μM. These results suggest that dMGer,
207 but not (−)-GR24, binds to the ligand binding pocket of D14L.

208 We also examined the binding of these compounds to D14L using DSF. D14L showed no
209 Tm shift upon addition of (−)-GR24 (Figure 2B). In contrast, D14L showed a clear, dose-

210 dependent decrease in Tm upon addition of dMGer (Figure 2B), indicating the ability of dMGer
211 to directly interact with and change the structure of D14L.

212

213 **dMGer enhances the direct interactions of D14L with D3 and OsSMAX1**

214 We next examined the interactions between the KL signaling components *in vitro*. We first
215 performed pull-down assays using maltose-binding protein (MBP)-tagged D3 (MBP-D3) and
216 Glutathione-S-transferase (GST)-tagged D14L. We found that MBP-D3, but not the control
217 protein MBP-hexahistidine (His), interacted weakly with GST-D14L in the absence of KL
218 analogs. This interaction was enhanced by dMGer, but not by (−)-GR24 (Figure 3A). We then
219 performed pull-down assays using MBP-His-OsSMAX1 and GST-D14L. These proteins
220 interacted even in the absence of KL analogs, and their interaction was also strengthened by
221 the addition of dMGer (Figure 3B). In addition, the pull-down assay using MBP-D3 and GST-
222 OsSMAX1 showed an interaction between these proteins in the absence of KL analogs (Figure
223 3C). These results demonstrate that the components of the KL signaling pathway are capable
224 of directly interacting with one another *in vitro* and that dMGer enhances the interactions of
225 D14L with D3 and OsSMAX1, suggesting its critical role in promoting the assembly of the KL
226 signaling complex.

227

228 **Domains of OsSMAX1 and D53 differentially interact with D14L or D14**

229 As we demonstrated the interaction of D14L and OsSMAX1 and the enhancement of the
230 interaction by dMGer *in vitro*, we next examined the functions of the domains of OsSMAX1.
231 To compare the affinity of the OsSMAX1 D1M and D2 domains to D14L, we pulled down
232 GST-D14 using MBP-His-OsSMAX1-D1M or MBP-His-OsSMAX1-D2. The D1M domain
233 showed a stronger interaction with D14L than the D2 domain. While dMGer enhanced the
234 interaction of the D1M domain with D14L, it did not enhance the interaction of the D2 domain
235 with D14L (Figure 3B). As it has been shown that D3-CTH enhances the interaction between
236 the D53-D2 domain and D14 (Shabek et al., 2018), we examined whether D3-CTH enhances
237 the interaction between the OsSMAX1-D2 domain and D14L. However, D3-CTH did not
238 enhance the interaction between OsSMAX1-D2 domain and D14L either in the absence or

239 presence of dMGer (Figure 3D). We also examined the interaction of the OsSMAX1 domains
240 with D3. The pull-down assay showed an interaction between OsSMAX1-D1M and D3 (Figure
241 3C). These results demonstrate that the OsSMAX1-D1M domain plays a central role in the
242 interaction of OsSMAX1 with D14L and D3.

243 As our results suggested that the functions of OsSMAX1 domains for the interaction with
244 D14L are different from those of D53 domains for the interaction with D14, we investigated
245 the interactions of OsSMAX1 and D53 domains with D14L and D14. In our *in vitro* pull-down
246 assays, D14L strongly interacted with the OsSMAX1-D1M domain, while it hardly interacted
247 with the D53-D1M domain in the presence of dMGer. Although OsSMAX1-D2 and D53-D2
248 domains seem to have similar levels of affinity for D14L, these interactions were much weaker
249 than the interaction between D14L and the OsSMAX1-D1M domain (Figure 4A). In contrast,
250 D14 showed a stronger interaction with the D53-D2 domain in the presence of the D14 ligand
251 (+)-GR24 than with the interactions with D53-D1M, OsSMAX1-D1M, and OsSMAX1-D2
252 domains (Figure 4B). This D14–D53-D2 interaction was enhanced by D3-CTH in a manner
253 consistent with the previous report (Shabek et al., 2018). D3-CTH also increased the interaction
254 efficiency between D14 and the OsSMAX1-D2 domain. The affinities of D14 with the two D2
255 domains in the presence of D3-CTH did not show any apparent difference (Figure 4B). These
256 results suggest that D14–D53 and D14L–OsSMAX1 complexes exhibit distinct binding modes.

257

258 **Discussion**

259 Although the model of the KL signaling pathway, in which its components interact in a ligand-
260 dependent manner, is widely accepted, the ligand-dependent interactions among these
261 components have not been fully demonstrated. Using the recently developed artificial KL
262 analog, dMGer, we addressed this issue. We show that dMGer effectively and selectively
263 induces KL responses in rice and directly interacts with D14L. Furthermore, we demonstrate
264 that the direct interaction between D3 and D14L is induced by dMGer, but not by (−)-GR24.
265 We also report, for the first time, the enhancement of the interaction between D14L/KAI2 and
266 SMAX1 by KL analogs *in vitro*. These findings demonstrate that these three proteins directly
267 interact in a KL-responsive manner. Furthermore, parallel comparisons of interactions of D14L
268 and D14 with domains of SMXL and D53 revealed regions that contribute to the specificity of

269 KL and SL signaling. Collectively, our findings advance the understanding of the KL signaling
270 by addressing knowledge gaps regarding the ligand perception and the interactions among the
271 signaling components.

272 This work is the first report describing the physiological responses of rice to desmethyl-
273 type KL analogs. dMGer has been shown to suppress hypocotyl elongation in a KAI2-
274 dependent manner and to induce seed germination; however, evaluation of its physiological
275 activities has been largely limited to Arabidopsis, except for germination-induction assays with
276 the root parasitic plants *Orobanche minor* and *Striga hermonthica*, in which KAI2-dependency
277 was not examined (Okabe et al., 2023). In the case of other desmethyl-type analogs, their
278 physiological activity has been investigated only in Arabidopsis and *Brachypodium distachyon*
279 (Yao et al., 2021; Meng et al., 2022). The observed D14L-dependent effects on plant growth,
280 the regulation of KL marker genes, and the protein levels of OsSMAX1 demonstrate the
281 function of dMGer as a KL analog in rice, suggesting the potential of desmethyl-type analogs
282 in a wide range of species.

283 In our *in vitro* assays, dMGer and (−)-GR24 exhibited distinct activities. dMGer inhibited
284 dYLG hydrolysis by D14L and induced a Tm shift of D14L in DSF assays, indicating direct
285 binding to the D14L ligand-binding pocket and induction of structural changes in D14L,
286 whereas (−)-GR24 did not induce these responses. Consistently, dMGer, but not (−)-GR24,
287 enhanced the interaction between D14L and D3. Similarly, in Arabidopsis, although (−)-GR24
288 induces a slight Tm shift of KAI2 in DSF assay, the shift is much weaker than that induced by
289 a desmethyl-type KL analog dGR24 (Yao et al., 2021). (−)-GR24 only marginally enhanced
290 the interaction between KAI2 and MAX2 *in vitro* (Xu et al., 2018). These results imply that
291 the *in vitro* activity of (−)-GR24 toward Arabidopsis KAI2 is also limited. The use of
292 desmethyl-type KL analogs may also reveal the interaction of the KL signaling components in
293 Arabidopsis.

294 Despite the lack of *in vitro* activity of (−)-GR24 toward D14L, it induces KL responses in
295 rice. Several possible explanations could account for the discrepancy between the *in vitro* and
296 *in vivo* activities of (−)-GR24. One explanation is the requirement for *in vivo* conversion of
297 (−)-GR24 into an active molecule, as suggested in the case of KARs. Previous studies
298 demonstrated that neither KAR_1 nor KAR_2 shifts the Tm of KAI2 in DSF assays, and that
299 KAR_1 is slow to induce ubiquitination of SMXL2 (Waters et al., 2015; Wang et al., 2020b).
300 These findings suggest that metabolic processing renders KARs active. (−)-GR24 may likewise

301 undergo metabolic conversion into an unidentified bioactive form *in vivo*. An alternative
302 hypothesis is that KAI2/D14L is subject to post-translational modifications that alter its mode
303 of ligand recognition. Various enzymatic and non-enzymatic post-translational modifications
304 that influence catalytic activity or protein folding have been documented (Kokkinidis et al.,
305 2020). Another possibility is that D14L recognizes (−)-GR24 only in the presence of plant-
306 derived cofactors. As an example of cofactor requirements in plant hormone signaling, binding
307 of inositol pentakisphosphate is essential for CORONATINE INSENSITIVE 1 and JAZ
308 proteins to function as the co-receptor of jasmonate (Sheard et al., 2010).

309 Taking advantage of the *in vitro* activity of dMGer, we characterized the interaction mode
310 of the KL signaling components. In the absence of dMGer, although the interaction between
311 D3 and D14L was hardly detectable, both D3 and D14L interacted with OsSMAX1, indicating
312 that D14L, D3, and OsSMAX1 can form a complex even in the absence of the ligand. In the
313 presence of dMGer, the interactions of D14L with D3 and OsSMAX1 were enhanced. These
314 results suggest that the function of KL is not to assemble three spatially separated components
315 into a single complex, but rather to modulate interactions within the complex, presumably
316 inducing conformational changes required for the ubiquitination of OsSMAX1, although
317 further *in vivo* evaluation is required to confirm this model (Figure 5A).

318 Furthermore, we clarified differences in the mode of interaction between the KL and SL
319 signaling complexes. The selective interaction of D14L with OsSMAX1 relies on its strong
320 affinity to the OsSMAX1-D1M domain rather than the D2 domain. On the other hand, D14
321 prefers the D53-D2 domain rather than the D1M domain. D3-CTH enhances the interaction
322 between D14 and D53-D2, but not the interaction between D14L and OsSMAX1-D2 (Figure
323 5B). Previous studies have shown that D3/MAX2-CTH is involved in the KL signaling (Tal
324 et al., 2022; Tal et al., 2023). Our results suggest that D3/MAX2-CTH functions in the KL
325 signaling pathway are different from those in the SL signaling. These findings demonstrate that
326 although D14 and D14L, as well as D53 and OsSMAX1, are paralogs, they distinctively
327 interact in the KL and SL signaling complexes. Intriguingly, D3-CTH also enhanced the
328 interaction of D14 with OsSMAX1-D2 under our assay conditions. Previously, the *in vivo*
329 interaction between AtD14 and SMAX1/SMXL2 has been reported (Wang et al., 2020b; Li et
330 al., 2022). This interaction may be mediated by the SMAX1-D2 domain and D3/MAX2-CTH.
331 Further biochemical and structural dissection of SMAX1 and D53 domains would elucidate
332 the molecular basis underlying the divergence of the KL and SL signaling pathways.

333

334 **Materials and Methods**

335 **Plant materials and growth conditions**

336 The rice cultivar Nipponbare was used as the wild type. The *d14l-c1* line was previously
337 described (Mashiguchi et al., 2023). The *d14l-c2* line was generated using the same gRNA as
338 that for *d14l-c1*, as described previously (Mashiguchi et al., 2023). Due to the duplication of
339 the 174th cytosine in the D14L ORF, a frame shift occurs after the 59th amino acid residue,
340 generating a premature stop codon. The previously described *d14l-1* line in the Nipponbare
341 genetic background (Zheng et al., 2020) was used for the protein degradation assay.

342 To test mesocotyl responses to dMGer, rice seeds were surface-sterilized with sodium
343 hypochlorite for 15 minutes and placed on 0.6% (w/v) agarose plates supplemented with the
344 indicated concentrations of the compounds. A 1000× stock solution of dMGer, dissolved in
345 acetone, was added to the medium to achieve the final concentrations. Plates containing 0.1%
346 acetone served as mock controls. Seeds were germinated and grown in the dark at 28 °C for 8
347 days in an incubator. To remove seedlings that did not germinate properly from the analysis,
348 only seedlings that properly developed embryonic roots and had a ≥2-cm of aerial part were
349 measured. Mesocotyl length was measured using Fiji.

350 To test the effects of chemicals on *DLK2b* and *KUF1* transcription, rice seeds were surface-
351 sterilized with sodium hypochlorite for 15 minutes and then grown on solid Hoagland medium
352 containing 0.8% Phytagel for 4 days at 28 °C under a 12-h light/12-h dark cycle. Uniform
353 seedlings were then selected and transferred to 1 mL of Hoagland solution, cultured overnight,
354 and then incubated for 6 hours with 0.1, 1, or 10 μM of (−)-GR24 or dMGer at 28°C. A 1000×
355 stock solution of each compound, dissolved in acetone, was used to achieve the final
356 concentrations. Hoagland solution containing 0.1% (v/v) acetone without any added compound
357 was used as the mock control.

358 Primary calli of WT and the *d14l-1* mutants (Zheng et al., 2020) for protein degradation assay
359 were induced on solid induction medium at 28°C under a photoperiod of 22 hours light
360 followed by 2 hours dark for a duration of 10 days (Jiang et al., 2013). Subsequently, the
361 primary calli were transferred onto plates containing solid induction medium for subculturing.

362 The calli were maintained on these plates for a maximum of 14 days, after which they required
363 transfer to fresh plates to ensure continued growth.

364

365 **qRT-PCR analysis**

366 Total RNA was extracted from rice roots using the EasyPure Plant RNA Kit (TransGen). An
367 aliquot (0.05–0.2 μg) was used for first-strand cDNA synthesis with the TransScript Uni All-
368 in-One First-Strand cDNA Synthesis SuperMix for qPCR (TransGen). RT-qPCR was
369 performed using gene-specific primers (Supplementary Table S1) on an Agilent Mx3000P
370 system, following the manufacturer's instructions. Each 10 μL reaction contained 1 μL of
371 diluted cDNA, 0.2 μM of each primer, and 5 μL of KOD SYBR qPCR Mix (Toyobo). The rice
372 *UBQ* gene was used as an internal reference.

373

374 **Protein degradation assay**

375 Twice sub-cultured calli were collected and divided into separate 10 ml tubes containing 3 ml
376 fresh liquid induction medium, then incubated at 28°C on orbital shaker (80 rpm) for 2 hours.
377 After this pre-incubation, dMGer, or (−)-GR24 at specified concentrations were added to the
378 samples for treatment. Following the treatment for two hours, callus samples were quickly
379 collected and immediately frozen in liquid nitrogen. The stock solution of dMGer and (−)-
380 GR24 were prepared by dissolving them in acetone. Acetone without any added compound was
381 used as the mock control.

382 For protein extraction, the frozen samples were ground into powder. Protein extraction buffer
383 (50 mM Tris-HCl, pH 7.5, 150 mM NaCl, 5 mM EDTA, 1% Triton X-100, 0.5% (w/v) SDS,
384 0.5% β-mercaptoethanol, 50 μM MG132, 5 mM DTT, 1× protease inhibitor cocktail, and 1
385 mM PMSF) was added to the powdered callus tissue. The mixture was vortexed for 30 seconds
386 and then incubated on ice for 2 minutes; this process was repeated five times to ensure complete
387 cell lysis. The lysate was centrifuged at 12,000 rpm for 10 minutes at 4°C, and the supernatant
388 was collected. Subsequently, 5×SDS loading buffer was added to the supernatant, which was
389 then heated at 95°C for 10 minutes to denature the proteins.

390 Proteins were separated by SDS-PAGE and transferred onto PVDF membranes. Detection of
391 OsSMAX1 was performed as described by Zheng et al. (2020), using polyclonal antibodies
392 against OsSMAX1 at a 1:5000 dilution. ACTIN was used as internal loading controls and
393 detected with anti-ACTIN (1:5000) antibody (Abclonal).

394

395 **Plasmid construction**

396 To construct the plasmid for expressing His-D14L for DSF assays, the ORF fragment of *D14L*
397 was amplified by PCR from cDNA synthesized from rice total RNA. The PCR product was
398 cloned by In-Fusion (Takarabio) into the pET47b vector (Novagen) using SmaI and SacI sites.
399 To construct the plasmid for expressing MBP-His-D14L, the CDS of *D14L* was amplified from
400 cDNA synthesized from rice total RNA, and the PCR product was inserted into the Sma1 and
401 EcoR1 sites of the modified pMAL-c5x vector (Seto et al., 2019) (pMALHis). For expression
402 of GST-D14L, the *D14L* CDS was subcloned from pMALHis-D14L into pGEX-4T-3 (Cytiva)
403 using EcoRI and NotI sites. For expression of GST-D14, the *D14* (50–318) CDS in cDNA
404 synthesized from rice total RNA was amplified and inserted into pGEX-4T-3 using EcoRI and
405 NotI sites.

406 For the bacterial expression of MBP-His-tagged full-length OsSMAX1 (residues 2–1041)
407 (OsSMAX1-FL) and domains of OsSMAX1 (D1M: 218–541; D2: 638–1041), the
408 corresponding CDS regions were amplified from cDNA synthesized from rice total RNA. PCR
409 products were first inserted into pGEX-4T-3, followed by subcloning into pMALHis, replacing
410 D14L in pMALHis-D14L.

411 For the bacterial expression of MBP-His-tagged domains of D53, the fragments encoding the
412 D1M (182–510) and D2 (718–1131) domains of D53 were amplified from rice genomic DNA.
413 The D53-D1M fragment was produced by overlap extension PCR using two fragments
414 amplified from exon 1 and exon 2 of genomic *D53*. A nonsynonymous substitution found in
415 the amplified D53-D1M fragment was corrected by overlap extension PCR. These fragments
416 were cloned into pMALHis.

417

418 To construct a plasmid for co-expression of MBP-tagged D3 (2–720) and untagged ASK1 in

419 insect cells, the CDSs of *D3* and *ASK1* were amplified from cDNA synthesized from total RNA
420 extracted from rice and Arabidopsis seedlings, respectively. ASK1 was inserted into pFastBac
421 Dual (Thermo Fisher Scientific) at the *Nco*I site downstream of the p10 promoter, yielding
422 pFastBacDual-ASK1. *D3* was first cloned into pGEX-4T-3 and then subcloned into
423 pFastBacDual-ASK1 downstream of the polyhedrin promoter, fused with an MBP tag
424 amplified from pMALHis. For multi-fragment assembly, we used the ClonExpress II One Step
425 Cloning Kit (Vazyme).

426 Primers used for the plasmid construction are listed in Supplementary Table S1.

427 **Preparation of recombinant proteins**

428 *E. coli* BL21(DE3) was used for the expression of D14L for DSF. The overnight culture (20
429 mL) was added to a fresh LB medium (2.0 L) containing kanamycin (50 mg/L) at 37ºC. After
430 OD600 reached 0.8, 0.25 mM isopropyl β-D-1-thiogalactopyranoside (IPTG) was added, and
431 the culture was further incubated at 18 °C for 21 h. The culture medium was centrifuged at
432 3500 *g* and the pellet was stored at −30ºC until use. The pellet was resuspended and sonicated
433 in lysis buffer (50 mM Tris buffer (pH 8.0) containing 500 mM NaCl, 5 mM 2-
434 mercaptoethanol, and 10 % glycerol). The supernatant was purified using His60 Ni
435 Superflow Resin (1 mL, Takara). After washing with the washing buffer (50 mM Tris buffer
436 (pH 8.0) containing 500 mM NaCl and 20 mM imidazole), the bound protein was eluted with
437 elution buffer (50 mM Tris buffer (pH 8.0) containing 500 mM NaCl and 200 mM
438 imidazole). The eluate was concentrated using VIVASPIN Turbo 15 (Sartorius), adjusted to
439 12 mg/mL, aliquoted, immediately frozen in liquid nitrogen, and stored at −80ºC until use.

440 *E.coli* strain Rosetta (DE3) (Novagen) was used for the production of recombinant proteins,
441 except for D3 and ASK1, for *in vitro* pull-down assays and dYLG assays. Transformed cells
442 were cultured in LB media containing 50 μg/mL carbenicillin and 50 μg/mL chloramphenicol
443 at 16 °C until the OD_{600} reached 0.4–0.6. Protein expression was induced with 0.1 mM IPTG,
444 and cells were incubated overnight at 16 °C.

445 For purification of MBP-6×His-fused D14L, OsSMAX1-D1M, OsSMAX1-D2, OsSMAX1-
446 FL, D53-D1M, D53-D2, and the MBP-6×His control protein, cells were harvested by
447 centrifugation and lysed by sonication in lysis buffer (25 mM Tris-HCl, pH 8.0, 500 mM NaCl,
448 1 mM TCEP, 20 mM imidazole, and 0.4 mM phenylmethylsulfonyl fluoride (PMSF)). The
449 lysate was centrifuged at 18,000 rpm for 50 min at 4 °C. The supernatant was applied to Ni

450 NTA Beads (Smart-Lifesciences) in a Poly-Prep Chromatography Column (Bio-Rad). After
451 washing with lysis buffer, proteins were eluted with MBP elution buffer (20 mM Tris-HCl,
452 pH 8.0, 500 mM NaCl, 1 mM TCEP, and 250 mM imidazole). The eluate was subsequently
453 applied to Dextrin Beads (Smart-Lifesciences) in a Poly-Prep Chromatography Column. After
454 washing with MBP wash buffer (20 mM Tris-HCl, pH 8.0, 500 mM NaCl, 1 mM TCEP),
455 proteins were eluted with MBP elution buffer (MBP wash buffer containing 10 mM maltose).
456 Eluted proteins were concentrated and subjected to buffer exchange using Amicon Ultra-15
457 (10 kDa MWCO for MBP-6×His, 30 kDa for the others). The buffer was exchanged first to
458 MBP wash buffer, and then to either 50 mM Tris-HCl, pH 7.6, 150 mM NaCl, 0.5 mM TCEP
459 (for D14L), 20 mM Tris-HCl, pH 7.5, 500 mM NaCl, 0.5 mM TCEP (for OsSMAX1-D1M,
460 and D53-D1M), 50 mM Tris-HCl, pH 7.5, 500 mM NaCl, 0.5 mM TCEP (for OsSMAX1-D2
461 and D53-D2), or 20 mM Tris, pH 8.0, 500 mM NaCl, 0.5 mM TCEP (for OsSMAX1-FL, MBP-
462 6xHis). In the final dialyzed samples, the residual concentrations of MBP elution and MBP
463 wash buffers were less than 0.2% and 1% (v/v), respectively.

464 For purification of GST-D14L and GST-D14, cells were harvested by centrifugation and lysed
465 by sonication in lysis buffer (25 mM Tris-HCl, pH 7.6, 500 mM NaCl, 1 mM TCEP, and
466 0.4 mM PMSF). The lysate was centrifuged at 18,000 rpm for 50 min at 4 °C. The supernatant
467 was applied to Glutathione Beads (Smart-Lifesciences) packed in a Poly-Prep Chromatography
468 Column. After sequential washing with lysis buffer and GST wash buffer (100 mM Tris-HCl,
469 pH 8.0, 500 mM NaCl, 1 mM TCEP), proteins were eluted with GST elution buffer (100 mM
470 Tris-HCl, pH 8.0, 500 mM NaCl, and 20 mM reduced glutathione). Eluted proteins were
471 concentrated and subjected to buffer exchange using Amicon Ultra-15 centrifugal filters
472 (30 kDa MWCO). The buffer was first exchanged to dialysis buffer 1 (100 mM Tris-HCl,
473 pH 8.0, 500 mM NaCl, 0.5 mM TCEP), and then to 50 mM Tris-HCl, pH 7.5, 150 mM NaCl,
474 0.5 mM TCEP. In the final dialyzed samples, the residual concentrations of GST elution and
475 dialysis buffer 1 were less than 0.2% and 1% (v/v), respectively.

476 For purification of GST-fused OsSMAX1-D1M, OsSMAX1-D2, and OsSMAX1-FL, the same
477 lysis, GST wash, and GST elution buffers as those for the purification of GST-D14L and GST-
478 D14 were used. For OsSMAX1-D1M and OsSMAX1-FL, the sonicated cell lysate was mixed
479 with polyethylenimine (Sinopharm Chemical Reagent Co., Ltd) to a final concentration of
480 approximately 0.1%(w/v) before centrifugation at 18,000 rpm. Subsequent purification with
481 Glutathione Beads was similar to that for GST-D14L/D14. Eluted proteins were concentrated

482 and subjected to buffer exchange using Amicon Ultra-15 centrifugal filters (30 kDa MWCO).
483 The buffer was first exchanged to dialysis buffer 1, and then to either 50 mM HEPES-NaOH,
484 pH 7.0, 500 mM NaCl, 0.5 mM TCEP (for D1M and FL) or 50 mM HEPES-NaOH, pH 7.0,
485 500 mM NaCl, 1 mM TCEP (for D2).

486 MBP-tagged D3 was co-expressed with untagged ASK1 in *Spodoptera frugiperda* Sf9 cells.
487 Suspension cultures were infected with recombinant baculovirus generated using the Bac-to-
488 Bac Baculovirus Expression System (Thermo Fisher Scientific), following the manufacturer's
489 instructions. Cells were harvested by centrifugation and lysed by sonication in 50 mM Tris-
490 HCl, pH 7.5, 200 mM NaCl, 0.5 mM TCEP, 1% Protease Inhibitor Cocktail (EDTA-Free)
491 (APExBIO, K1007). The lysate was clarified by centrifugation at 18,000 rpm for 50 min at
492 4 °C, and the supernatant was applied to Dextrin Beads (Smart Lifesciences) in a Poly-Prep
493 chromatography column (Bio-Rad). After washing with D3 wash buffer (50 mM Tris-HCl,
494 pH 7.5, 200 mM NaCl, 0.5 mM TCEP), bound proteins were eluted with D3 elution buffer (D3
495 wash buffer supplemented with 10 mM maltose). Eluted proteins were concentrated and
496 subjected to buffer exchange using Amicon Ultra-4 (10 kDa MWCO). The buffer was first
497 exchanged to D3 wash buffer, followed by 50 mM Tris-HCl, pH 7.5, 150 mM NaCl, 0.5 mM
498 TCEP. In the final dialyzed samples, the residual concentrations of D3 elution and D3 wash
499 buffers were less than 0.1% and 1% (v/v), respectively.

500

501 **Differential scanning fluorometry experiments**

502 DSF was conducted using 4.8 μg of the recombinant D14L protein in 20 μL of PBS buffer
503 containing the 0.005 μL of Sypro Orange (Ex/Em: 490/610 nm; Invitrogen) and the tested
504 compound with 5% (v/v) acetone on a 96-well plate. Mixtures were heated from 20ºC to 95ºC,
505 and the fluorescence (Ex/Em; 490/610) was continuously scanned by using LightCycler480.
506 The denaturation curve was calculated by using the LightCycler480 Software.

507

508 **dYLG hydrolysis assays**

509 Reactions contained 1 μM dYLG, 0–5 μM competitor, 0.3% DMSO, and 10 μg/mL MBP-
510 6×His-D14L. Recombinant protein (10 mg/mL in 50 mM Tris-HCl, pH 7.6, 150 mM NaCl,
511 0.5 mM TCEP) was diluted 500-fold with reaction buffer (100 mM HEPES, pH 7.0, 150 mM

512 NaCl). dYLG (1 mM stock in DMSO) and the competitor (500× stock in DMSO) were diluted
513 with reaction buffer to twice their final concentrations before addition to the reaction. Protein
514 solution (25 μL/well) was dispensed into a 1/2 Area OptiPlate-96 (PerkinElmer), followed by
515 the addition of an equal volume of the dYLG/competitor solution, on ice. Fluorescence
516 intensity was measured at 30 °C in the dark (Ex/Et: 480/520 nm) using Varioskan Flash
517 (Thermo Fisher Scientific).

518

519 **Pull-down assays**

520 The of D14L with D3 or domains of OsSMAX1/D53 were assessed using 2.5 μg GST-D14L
521 (prey protein) was incubated with an approximately equimolar MBP-His (as a control) or
522 MBP-tagged bait proteins at 4 °C in 700 μL of incubation buffer (20 mM Bis-Tris-HCl,
523 pH 7.0, 150 mM NaCl, 0.1% Triton X-100, 0.2% DMSO for D3; 20 mM Tris-HCl, pH 7.5,
524 150 mM NaCl, 0.1% Triton X-100, 0.2% DMSO for the others). After ~1 h of incubation,
525 25 μL of 50% Dextrin Beads (Smart Lifesciences) slurry, equilibrated and suspended in
526 incubation buffer without KL analog, were added and incubated at 4 °C for ~1.5 h. Beads
527 were washed three times with incubation buffer, and bound proteins were eluted with elution
528 buffer (20 mM Bis-Tris-HCl, pH 7.0, 150 mM NaCl, 10 mM maltose for D3; 20 mM Tris-
529 HCl, pH 7.5, 150 mM NaCl, 10 mM maltose for the others). Eluates were mixed with an
530 equal volume of 2× SDS-PAGE sample buffer and boiled at 95 °C for 5 min. To test the
531 effects of dMGer or (−)-GR24, 10 μM of each chemical was added to the incubation buffer.
532 When testing the effects of D3-CTH, synthesized D3-CTH peptideswere added at an
533 approximately equimolar to the prey protein, and the beads were washed with incubation
534 buffer containing no peptide.

535 The interactions of D14 with domains of OsSMAX1/D53 were assessed using similar
536 procedures to those for D14L. 10 μM (+)-GR24 was added to the incubation buffer (20 mM
537 Tris-HCl, pH 7.5, 150 mM NaCl, 0.1% Triton X-100, 0.2% DMSO).

538 To assess the interactions between D3 and domains of OsSMAX1, 5 μg of MBP-D3-ASK1
539 and 2 μg of MBP-6×His (control) were incubated with an approximately equimolar amounts
540 of GST-tagged bait proteins or GST (control) in 700 μL of incubation buffer (20 mM Tris-HCl,
541 pH 7.5, 150 mM NaCl, 0.5 mM TCEP, 0.1% Triton X-100). After ~1 h of incubation, 25 μL of
542 50% Glutathione Beads (Smart Lifesciences) slurry, equilibrated and suspended in incubation

543 buffer, was added and incubated at 4 °C for ~1.5 h. Beads were washed three times with
544 incubation buffer, and bound proteins were eluted with elution buffer (100 mM Tris-HCl,
545 pH8.0, 150 mM NaCl, 20 mM Reduced glutathione). Eluates were mixed with an equal volume
546 of 2× SDS-PAGE sample buffer and boiled at 95 °C for 5 min.

547 Input and eluted proteins were resolved by SDS-PAGE and detected by western blotting.
548 Western blots were performed using mouse anti-GST antibody (Beijing Protein Innovation,
549 AbM59001-2H5-PU; 1:3000–1:1000 diluted), mouse anti-MBP antibody (Beijing Protein
550 Innovation, AbM59007-3-PU; 1:6000–1:1000 diluted), and HRP-conjugated goat anti-mouse
551 IgG (H+L) (ABclonal, AS003; 1:10000 diluted).

552

553 **Funding**
554 This research was supported by the Key Laboratory of Plant Carbon Capture, Chinese
555 Academy of Sciences.

556

557 **Author contributions**

558 H.K. and K.T. designed the research. K.T., J.W., Q.X., Y.H., T.S., Y.Y., Y.S., and G.X.
559 performed research. K.T., J.W., Q.X, Y.H., T.S., Y.S., G.X., and H.K. analyzed data. K.T. and
560 H.K. wrote the manuscript.

561

562 **Acknowledgements**
563 We thank to Miaolian Ma (Eukaryotic Protein Expression and Purification Platform, CAS
564 CEMPS) for technical support in protein expression using insect cell culture, Liu Li (Core
565 Facility Center of CEMPS, CAS) for technical instruction on fluorescence measurements, Prof.
566 Dr. Minrui Fan (CAS CEMPS) for access to the equipment for protein extraction, Prof. Dr.
567 Ruiqiang Ye (CAS CEMPS) for access to the equipment for western blot, and Dr. Kosuke Fukui
568 (Tokyo University of Science) for providing dMGer.

569

570 **Conflict of interest**

The authors declare no conflict of interests.

References

Abe, S., Sado, A., Tanaka, K., Kisugi, T., Asami, K., Ota, S., Kim, H. I., Yoneyama, K., Xie, X., Ohnishi, T., et al. (2014). Carlactone is converted to carlactonoic acid by MAX1 in *Arabidopsis* and its methyl ester can directly interact with AtD14 in vitro. *Proc. Natl Acad. Sci. U.S.A.* **111**:18084–18089.

Carbonnel, S., Das, D., Varshney, K., Kolodziej, M. C., Villaécija-Aguilar, J. A., and Gutjahr, C. (2020). The karrikin signaling regulator SMAX1 controls *Lotus japonicus* root and root hair development by suppressing ethylene biosynthesis. *Proc. Natl Acad. Sci. U.S.A.* **117**:21757–21765.

Chiwocha, S. D. S., Dixon, K. W., Flematti, G. R., Ghisalberti, E. L., Merritt, D. J., Nelson, D. C., Riseborough, J.-A. M., Smith, S. M., and Stevens, J. C. (2009). Karrikins: A new family of plant growth regulators in smoke. *Plant Science* **177**:252–256.

Choi, J., Lee, T., Cho, J., Servante, E. K., Pucker, B., Summers, W., Bowden, S., Rahimi, M., An, K., An, G., et al. (2020). The negative regulator SMAX1 controls mycorrhizal symbiosis and strigolactone biosynthesis in rice. *Nat. Commun.* **11**:2114. https://doi.org/10.1038/s41467-020-16021-1

Conn, C. E., and Nelson, D. C. (2016). Evidence that KARRIKIN-INSENSITIVE2 (KAI2) Receptors may Perceive an Unknown Signal that is not Karrikin or Strigolactone. *Front. Plant Sci.* **6**. https://doi.org/10.3389/fpls.2015.01219.

de Saint Germain, A., Clavé, G., Badet-Denisot, M.-A., Pillot, J.-P., Cornu, D., Le Caer, J.-P., Burger, M., Pelissier, F., Retailleau, P., Turnbull, C., et al. (2016). An histidine covalent receptor and butenolide complex mediates strigolactone perception. *Nat. Chem. Biol.* **12**:787–794.

Fukui, K., Arai, K., Kasahara, H., Asami, T., and Hayashi, K. (2019). Synthetic agonist of HTL/KAI2 shows potent stimulating activity for *Arabidopsis* seed germination. *Bioorg. Med. Chem. Lett.* **29**:2487–2492.

Gutjahr, C., Gobbato, E., Choi, J., Riemann, M., Johnston, M. G., Summers, W., Carbonnel, S., Mansfield, C., Yang, S.-Y., Nadal, M., et al. (2015). Rice perception of symbiotic arbuscular mycorrhizal fungi requires the karrikin receptor complex. *Science* **350**:1521–1524.

Hamiaux, C., Drummond, R. S. M., Janssen, B. J., Ledger, S. E., Cooney, J. M., Newcomb, R. D., and Snowden, K. C. (2012). DAD2 Is an α/β Hydrolase Likely to Be Involved in the Perception of the Plant Branching Hormone, Strigolactone. *Current Biology* **22**:2032–2036.

Jiang, L., Liu, X., Xiong, G., Liu, H., Chen, F., Wang, L., Meng, X., Liu, G., Yu, H., Yuan, Y., et al. (2013). DWARF 53 acts as a repressor of strigolactone signalling in rice. *Nature* **504**:401–405.

Kameoka, H., and Kyozuka, J. (2015). Downregulation of Rice *DWARF 14 LIKE* Suppress Mesocotyl Elongation *via* a Strigolactone Independent Pathway in the Dark. *J. Genet. Genomics* **42**:119–124.

Khosla, A., Morffy, N., Li, Q., Faure, L., Chang, S. H., Yao, J., Zheng, J., Cai, M. L., Stanga, J., Flematti, G. R., et al. (2020). Structure–Function Analysis of SMAX1 Reveals Domains That Mediate Its Karrikin-Induced Proteolysis and Interaction with the Receptor KAI2. *Plant Cell* **32**:2639–2659.

Kokkinidis, M., Glykos, N. M., and Fadouloglou, V. E. (2020). Catalytic activity regulation through post-translational modification: the expanding universe of protein diversity. *Adv. Protein Chem. Struct. Biol* **122**:97–125.

Kushihara, R., Nakamura, A., Takegami, K., Seto, Y., Kato, Y., Dohra, H., Ohnishi, T., Todoroki, Y., and Takeuchi, J. (2025). Structural requirements of KAI2 ligands for activation of signal transduction. *Proc. Natl Acad. Sci. U.S.A.* **122**:e2414779122. https://doi.org/10.1073/pnas.2414779122.

Li, W., Nguyen, K. H., Chu, H. D., Ha, C. V., Watanabe, Y., Osakabe, Y., Leyva-González, M. A., Sato, M., Toyooka, K., Voges, L., et al. (2017). The karrikin receptor KAI2 promotes drought resistance in *Arabidopsis thaliana*. *PLOS Genetics* **13**:e1007076. https://doi.org/10.1371/journal.pgen.1007076

Li, Q., Martín-Fontecha, E. S., Khosla, A., White, A. R. F., Chang, S., Cubas, P., and Nelson, D. C. (2022). The strigolactone receptor D14 targets SMAX1 for degradation in response to GR24 treatment and osmotic stress. *Plant Commun.* **3**:100303. https://doi.org/10.1016/j.xplc.2022.100303

Mashiguchi, K., Morita, R., Tanaka, K., Kodama, K., Kameoka, H., Kyozuka, J., Seto, Y., and Yamaguchi, S. (2023). Activation of Strigolactone Biosynthesis by the DWARF14-LIKE/KARRIKIN-INSENSITIVE2 Pathway in Mycorrhizal Angiosperms, but Not in *Arabidopsis*, a Non-mycorrhizal Plant. *Plant Cell Physiol.* **64**:1066–1078.

Meng, Y., Varshney, K., Incze, N., Badics, E., Kamran, M., Davies, S. F., Oppermann, L. M. F., Magne, K., Dalmais, M., Bendahmane, A., et al. (2022). *KARRIKIN INSENSITIVE2* regulates leaf development, root system architecture and arbuscular-mycorrhizal symbiosis in *Brachypodium distachyon*. *Plant J.* **109**:1559–1574.

Mizuno, Y., Komatsu, A., Shimazaki, S., Naramoto, S., Inoue, K., Xie, X., Ishizaki, K., Kohchi, T., and Kyozuka, J. (2021). Major components of the KARRIKIN INSENSITIVE2-dependent signaling pathway are conserved in the liverwort Marchantia polymorpha. *Plant Cell* **33**:2395–2411.

Niesen, F. H., Berglund, H., and Vedadi, M. (2007). The use of differential scanning fluorimetry to detect ligand interactions that promote protein stability. *Nat. Protoc.* **2**:2212–2221.

Okabe, S., Kitaoka, K., Suzuki, T., Kuruma, M., Hagihara, S., Yamaguchi, S., Fukui, K., and Seto, Y. (2023). Desmethyl type germinone, a specific agonist for the HTL/KAI2

receptor, induces the Arabidopsis seed germination in a gibberellin-independent manner. *Biochem. Biophys. Res. Commun.* **649**:110–117.

Sepulveda, C., Guzmán, M. A., Li, Q., Villaécija-Aguilar, J. A., Martinez, S. E., Kamran, M., Khosla, A., Liu, W., Gendron, J. M., Gutjahr, C., et al. (2022). KARRIKIN UP-REGULATED F-BOX 1 (KUF1) imposes negative feedback regulation of karrikin and KAI2 ligand metabolism in *Arabidopsis thaliana*. *Proc. Natl Acad. Sci. U.S.A.* **119**:e2112820119. https://doi.org/10.1073/pnas.2112820119

Seto, Y., Yasui, R., Kameoka, H., Tamiru, M., Cao, M., Terauchi, R., Sakurada, A., Hirano, R., Kisugi, T., Hanada, A., et al. (2019). Strigolactone perception and deactivation by a hydrolase receptor DWARF14. *Nat. Commun.* **10**:191. https://doi.org/10.1038/s41467-018-08124-7

Shabek, N., Ticchiarelli, F., Mao, H., Hinds, T. R., Leyser, O., and Zheng, N. (2018). Structural plasticity of D3–D14 ubiquitin ligase in strigolactone signalling. *Nature* **563**:652–656.

Sheard, L. B., Tan, X., Mao, H., Withers, J., Ben-Nissan, G., Hinds, T. R., Kobayashi, Y., Hsu, F.-F., Sharon, M., Browse, J., et al. (2010). Jasmonate perception by inositol-phosphate-potentiated COI1–JAZ co-receptor. *Nature* **468**:400–405.

Soundappan, I., Bennett, T., Morffy, N., Liang, Y., Stanga, J. P., Abbas, A., Leyser, O., and Nelson, D. C. (2015). SMAX1-LIKE/D53 Family Members Enable Distinct MAX2-Dependent Responses to Strigolactones and Karrikins in Arabidopsis. *Plant Cell* **27**:3143–59

Tal, L., Guercio, A. M., Varshney, K., Young, A., Gutjahr, C., and Shabek, N. (2023). C-terminal conformational changes in SCF-D3/MAX2 ubiquitin ligase are required for KAI2-mediated signaling. *New Phytol.* **239**:2067–2075.

Villaécija-Aguilar, J. A., Hamon-Josse, M., Carbonnel, S., Kretschmar, A., Schmidt, C., Dawid, C., Bennett, T., and Gutjahr, C. (2019). SMAX1/SMXL2 regulate root and root hair development downstream of KAI2-mediated signalling in Arabidopsis. *PLOS Genet.* **15**:e1008327. https://doi.org/10.1371/journal.pgen.1008327

Wang, L., Wang, B., Jiang, L., Liu, X., Li, X., Lu, Z., Meng, X., Wang, Y., Smith, S. M., and Li, J. (2015). Strigolactone Signaling in Arabidopsis Regulates Shoot Development by Targeting D53-Like SMXL Repressor Proteins for Ubiquitination and Degradation. *Plant Cell* **27**:3128–3142.

Wang, L., Wang, B., Yu, H., Guo, H., Lin, T., Kou, L., Wang, A., Shao, N., Ma, H., Xiong, G., et al. (2020a). Transcriptional regulation of strigolactone signalling in *Arabidopsis*. *Nature* **583**:277–281.

Wang, L., Xu, Q., Yu, H., Ma, H., Li, X., Yang, J., Chu, J., Xie, Q., Wang, Y., Smith, S. M., et al. (2020b). Strigolactone and Karrikin Signaling Pathways Elicit Ubiquitination and Proteolysis of SMXL2 to Regulate Hypocotyl Elongation in Arabidopsis. *Plant Cell* **32**:2251–2270.

Waters, M. T., Nelson, D. C., Scaffidi, A., Flematti, G. R., Sun, Y. K., Dixon, K. W., and Smith, S. M. (2012). Specialisation within the DWARF14 protein family confers distinct responses to karrikins and strigolactones in Arabidopsis. *Development* **139**:1285–1295.

Waters, M. T., Scaffidi, A., Moulin, S. L. Y., Sun, Y. K., Flematti, G. R., and Smith, S. M. (2015). A *Selaginella moellendorffii* Ortholog of KARRIKIN INSENSITIVE2 Functions in Arabidopsis Development but Cannot Mediate Responses to Karrikins or Strigolactones. *Plant Cell* **27**:1925–1944.

Xu, Y., Miyakawa, T., Nosaki, S., Nakamura, A., Lyu, Y., Nakamura, H., Ohto, U., Ishida, H., Shimizu, T., Asami, T., et al. (2018). Structural analysis of HTL and D14 proteins reveals the basis for ligand selectivity in Striga. *Nat. Commun.* **9**:3947. https://doi.org/10.1038/s41467-018-06452-2

Yao, J., Mashiguchi, K., Scaffidi, A., Akatsu, T., Melville, K. T., Morita, R., Morimoto, Y., Smith, S. M., Seto, Y., Flematti, G. R., et al. (2018). An allelic series at the *KARRIKIN INSENSITIVE 2* locus of *Arabidopsis thaliana* decouples ligand hydrolysis and receptor degradation from downstream signalling. *Plant J.* **96**:75–89.

Yao, J., Scaffidi, A., Meng, Y., Melville, K. T., Komatsu, A., Khosla, A., Nelson, D. C., Kyozuka, J., Flematti, G. R., and Waters, M. T. (2021). Desmethyl butenolides are optimal ligands for karrikin receptor proteins. *New Phytol.* **230**:1003–1016.

Yasui R, Seto Y, Ito S, Kawada K, Itto-Nakama K, Mashiguchi K, Yamaguchi S (2019) Chemical screening of novel strigolactone agonists that specifically interact with DWARF14 protein. *Bioorg. Med. Chem. Lett.* **29**: 938–942

Zheng, J., Hong, K., Zeng, L., Wang, L., Kang, S., Qu, M., Dai, J., Zou, L., Zhu, L., Tang, Z., et al. (2020). Karrikin Signaling Acts Parallel to and Additively with Strigolactone Signaling to Regulate Rice Mesocotyl Elongation in Darkness. *Plant Cell* **32**:2780–2805.

Zhou, F., Lin, Q., Zhu, L., Ren, Y., Zhou, K., Shabek, N., Wu, F., Mao, H., Dong, W., Gan, L., et al. (2013). D14–SCFD3-dependent degradation of D53 regulates strigolactone signalling. *Nature* **504**:406–410.

722 **Figure legends**

723

724 **Figure 1. Response of rice seedlings to (−)-GR24 and desmethyl germinone treatments.**

725 (**A**) Representative images of 8-day-old wild-type (WT) and *d14l-c2* seedlings treated with 1
726 μM desmethyl germinone (dMGer) or 0.1% (v/v) acetone as a control. Scale bars: 1 cm.

727 (**B**) Length of mesocotyls of WT and *d14l-c2* plants treated with or without dMGer. Circles
728 represent individual data points. Open squares indicate means of each treatment group. Sample
729 numbers are presented above the plot for each condition. For statistical analysis, Welch's t-test
730 with Bonferroni correction was performed comparing the control and dMGer-treated groups of
731 each genotype. Calculated *p*-values are presented above the plots for each genotype.

732 (**C**, **D**) Transcript levels of *DLK2b* (**C**) and *KUF1* (**D**) in 5-day-old WT rice roots treated with
733 varying concentrations of (−)-GR24 or dMGer, or with 0.1% (v/v) acetone as control (n = 6).
734 Values are expressed as fold change relative to the mean value of the control. Circles represent
735 individual data points; bars indicate means of replicates. For statistical analysis, Welch's t-test
736 with Bonferroni correction was performed comparing the groups treated with the same
737 concentration of (−)-GR24 or dMGer. Calculated *p*-values are presented above the plots for
738 each pair of the compared groups.

739 (**E**, **F**) Transcript levels of *DLK2b* (**E**) and *KUF1* (**F**) in 5-day-old WT and *d14l-c1* mutant
740 roots treated with 10 μM (−)-GR24 or dMGer (n = 6). Acetone (0.1% (v/v)) was used as the
741 control treatment. Values are expressed relative to the mean value of the control WT plants.
742 Circles represent individual data points; bars indicate means of triplicates. For statistical
743 analysis, Welch's t-test with Bonferroni correction was performed comparing the groups
744 treated with the same concentration of (−)-GR24 or dMGer. Calculated *p*-values are presented
745 above the plots for each pair of the compared groups.

746 (**G**) Levels of OsSMAX1 in calli of WT and *d14l* at two hours following treatment with dMGer
747 or (−)-GR24 at the indicated concentrations. OsSMAX1, D14L, and ACTIN proteins were
748 detected by immunoblotting with anti-OsSMAX1, anti-D14L, and anti-ACTIN antibodies,
749 respectively. Immunobloting with the same antibody was performed on a single membrane.

750 Alt text: Panels labeled A to G showing effects of KAI2 ligand analogs. A presents pictures of
751 rice mesocotyls treated with desmethyl germinone. B is a plot of mesocotyl length, with

752 statistic values. C and D are plots of marker gene expression levels in wild-type rice treated
753 with different concentrations of desmethyl germinone and (−)-GR24, with statistic values. E
754 and F are plots of marker gene expression levels in wild-type and *d14l* mutant rice treated
755 with these KAI2 ligand analogs, with statistic values. G is immunoblot showing effects of the
756 KAI2 ligand analogs on SMAX1 protein levels.

757

758 **Figure 2. Binding of (−)-GR24 and desmethyl germinone to D14L *in vitro*.**

759 (**A**) Inhibitory effects of dMGer and (−)-GR24 on dYLG hydrolysis by MBP-6×His-D14L.
760 Reactions contained 1 μM dYLG, 10 ng/μL protein, and the indicated concentrations of (−)-
761 GR24 or dMGer. Dimethyl sulfoxide without either compound served as the mock control.
762 Circles represent individual data points, expressed relative to the mean fluorescence intensity
763 of mock reactions; bars indicate means (n = 8).

764 (**B**) Differential scanning fluorimetry (DSF) of MBP-His-D14L in the presence of 0–100 μM
765 (−)-GR24 (left) or desmethyl germinone (dMGer) (right). Melting curves of the protein
766 incubated with the indicated concentrations of each compound are shown in different colors.
767 Each line represents a single replicate (triplicates for each concentration). Control experiments,
768 in which the protein was incubated without KL analogs, are shown in both plots.

769 Alt text: Panels labeled A and B. A is a graph showing the competitive inhibition of D14L
770 hydrolase activity by desmethyl germinone or (−)-GR24. B presents graphs showing the results
771 of differential scanning fluorimetry in the presence of the KAI2 ligand analogs.

772

773 **Figure 3. Interactions between KL signaling components.**

774 (**A**) *In vitro* MBP pull-down assay using dextrin agarose beads, with MBP-D3 co-expressed
775 with ASK1 or MBP-His tag alone as bait, and GST-D14L as prey. All reactions contained 0.2%
776 (v/v) DMSO as solvent for chemicals. Assays were supplemented with either 10 μM dMGer,
777 10 μM (−)-GR24, or DMSO only. Calculated molecular masses: GST-D14L, ~56 kDa; MBP-
778 D3, ~121 kDa; MBP-His tag, ~45 kDa.

779 (**B**) *In vitro* MBP pull-down assay using MBP-His-tagged full-length (FL) or domain fragments
780 of OsSMAX1 as bait, and GST-D14L as prey. Assays were performed with or without 10 μM
781 dMGer. For better visualization of GST-D14L pulled-down by each bait, images of the same

782 blot taken with different exposure times (short and long) are shown. Calculated molecular
783 masses: MBP-His-OsSMAX1 FL, ~154 kDa; MBP-His-OsSMAX1-D1M, ~79 kDa; MBP-
784 His-OsSMAX1-D2, ~90 kDa.

785 (**C**) *In vitro* GST pull-down assay using glutathione agarose beads, with GST-tagged FL or
786 domains of OsSMAX1 as bait, and MBP-D3 or MBP-His as prey. Calculated molecular
787 masses: GST-OsSMAX1 FL, ~135 kDa; GST-OsSMAX1-D1M, ~60 kDa; GST-OsSMAX1-
788 D2, ~71 kDa; GST tag, ~28 kDa.

789 (**D**) *In vitro* MBP pull-down assay using MBP-His-OsSMAX1-D2 as bait and GST-D14L as
790 prey, performed in the presence or absence of D3-CTH peptide, with or without 10 μM dMGer.

791 GST- and MBP(-His)-tagged proteins were detected by immunoblotting with anti-GST and
792 anti-MBP antibodies, respectively. The positions of size markers electrophoresed with the
793 samples are shown alongside each blot.

794 Alt text: Immunoblots labeled A to D showing physical interactions among D14L, D3, and
795 OsSMAX1 proteins. A shows interaction between D14L and D3 promoted by desmethyl
796 germinone. B shows interaction of D14L with full-length or D1M region of OsSMAX1 and
797 effects of desmethyl germinone on the interactions. C shows interaction between D3 and
798 OsSMAX1. D shows effect of D3-C-terminal helix on interaction between D14L and D2
799 domain of OsSMAX1.

800

801 **Figure 4. Differential interaction of D14L and D14 with domains of OsSMAX1 and D53.**
802 (**A**) *In vitro* MBP pull-down assay using MBP-His-tagged domains of D53 or OsSMAX1 as
803 bait, and GST-D14L as prey. All reactions contained 10 μM dMGer. Calculated molecular
804 masses: MBP-His-D53-D1M, ~80 kDa; MBP-His-D53-D2, ~91 kDa.

805 (**B**) *In vitro* MBP pull-down assay using MBP-His-tagged domains of D53 or OsSMAX1 as
806 bait, and GST-D14 as prey, performed in the presence or absence of D3-CTH. All reactions
807 contained 10 μM (+)-GR24. Calculated molecular masses: GST-D14 ~56 kDa.

808 GST- and MBP-His-tagged proteins were detected by immunoblotting with anti-GST and anti-
809 MBP antibodies, respectively. The positions of size markers electrophoresed with the samples
810 are shown alongside each blot.

811 Alt text: Immunoblots labeled A and B showing selective interactions between components of
812 the KAI2 ligand and strigolactone signaling pathway. A presents interactions of D14L with
813 domains of OsSMAX1 and D53, showing a stronger binding to D1M of OsSMAX1. B presents
814 interactions of D14 with the same protein domains, showing a higher interaction with D2 of
815 D53 enhanced by D3-C-terminal helix peptide.

816

817 **Figure 5. Interactions between rice KL signaling components and effects of KL.**

818 (**A**) Model of KL-triggered changes in protein–protein interactions. Even in the absence of KL,
819 OsSMAX1 interacts with both D14L and D3, potentially forming a single complex. KL
820 promotes direct binding between D14L and D3 and enhances the interaction between D14L
821 and OsSMAX1, likely stabilizing and altering the conformation of the complex, thereby
822 leading to the ubiquitination of OsSMAX1. Differences in interaction strength are indicated by
823 the thickness of grey lines.

824 (**B**) Schematic of physical interactions of rice D14L and D14 with domains of OsSMAX1 and
825 D53. D14L mainly interacts with OsSMAX1-D1M, whereas D14 mainly interacts with D53-
826 D2. D3-CTH enhances the interaction between D14 and the D53-D2 domain. Differences in
827 interaction strength are indicated by the thickness of grey lines.

828 Alt text: Graphical abstracts of models derived from study results, labeled A and B. A illustrates
829 how ligand perception by D14L leads to protein–protein interactions and signal transduction.
830 B illustrates differences in the interactions between receptors and suppressor proteins in the
831 KAI2 ligand and strigolactone signaling pathways.

832

833 **Supplementary data**

834 **Supplementary Figure S1. Structure of compounds used in this study.**

835 Chemical structures of desmethyl germinone (dMGer) (top left), desmethyl Yoshimulactone
836 Green (dYLG) (top right), (−)-GR24 (bottom left), and (+)-GR24 (bottom right).

837

838 **Supplementary Figure S2. Uncropped blots.**

839 (**A**) Full western blot images of Figure 3A.

840 (**B**) Full western blot images of Figure 3B.

841 (**C**) Full western blot images of Figure 3C.

842 (**D**) Full western blot images of Figure 3D.

843 (**E**) Full western blot images of Figure 4A.

844 (**F**) Full western blot images of Figure 4B.

845

846 **Supplementary Table S1. List of primers used in this study.**

847

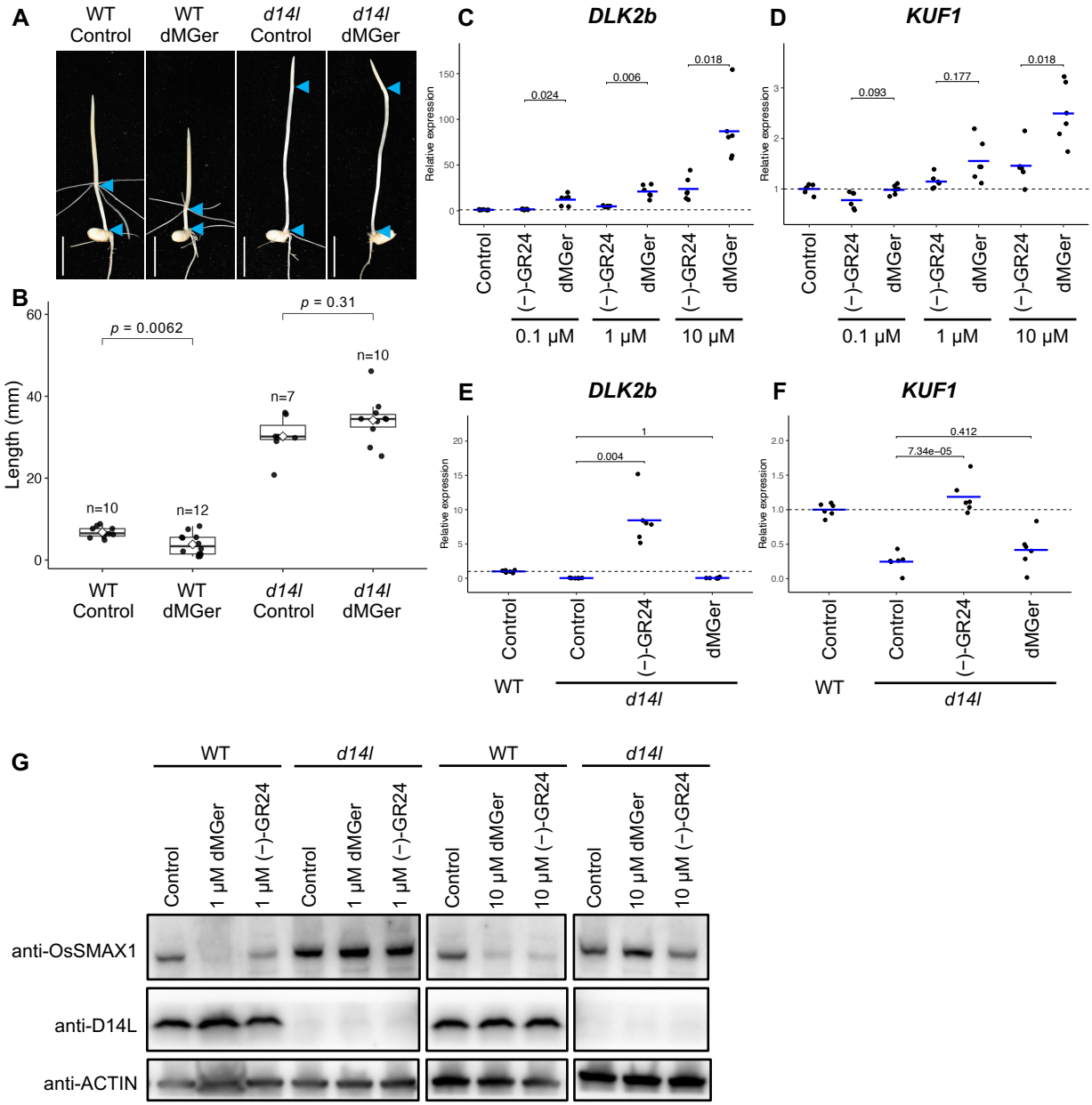

Figure 1. Response of rice seedlings to (−)-GR24 and desmethyl germinone treatments.
(**A**) Representative images of 8-day-old wild-type (WT) and *d14l-c2* seedlings treated with 1 μM desmethyl germinone (dMGer) or 0.1% (v/v) acetone as a control. Scale bars: 1 cm. (**B**) Length of mesocotyls of WT and *d14l-c2* plants treated with or without dMGer. Circles represent individual data points. Open squares indicate means of each treatment group. Sample numbers are presented above the plot for each condition. For statistical analysis, Welch's t-test with Bonferroni correction was performed comparing the control and dMGer-treated groups of each genotype. Calculated *p*-values are presented above the plots for each genotype. (**C**, **D**) Transcript levels of *DLK2b* (**C**) and *KUF1* (**D**) in 5-day-old WT rice roots treated with varying concentrations of (−)-GR24 or dMGer, or with 0.1% (v/v) acetone as control (n = 6). Values are expressed as fold change relative to the mean value of the control. Circles represent individual data points; bars indicate means of replicates. For statistical analysis, Welch's t-test with Bonferroni correction was performed comparing the groups treated with the same concentration of (−)-GR24 or dMGer. Calculated *p*-values are presented above the plots for each pair of the compared groups. (**E**, **F**) Transcript levels of *DLK2b* (**E**) and *KUF1* (**F**) in 5-day-old WT and *d14l-c1* mutant roots treated with 10 μM (−)-GR24 or dMGer (n = 6). Acetone (0.1% (v/v)) was used as the control treatment. Values are expressed relative to the mean value of the control WT plants. Circles represent individual data points; bars indicate means of triplicates. For statistical analysis, Welch's t-test with Bonferroni correction was performed comparing the groups treated with the same concentration of (−)-GR24 or dMGer. Calculated *p*-values are presented above the plots for each pair of the compared groups. (**G**) Levels of OsSMAX1 in calli of WT and *d14l* at two hours following treatment with dMGer or (−)-GR24 at the indicated concentrations. OsSMAX1, D14L, and ACTIN proteins were detected by immunoblotting with anti-OsSMAX1, anti-D14L, and anti-ACTIN antibodies, respectively. Immunobloting with the same antibody was performed on a single membrane.

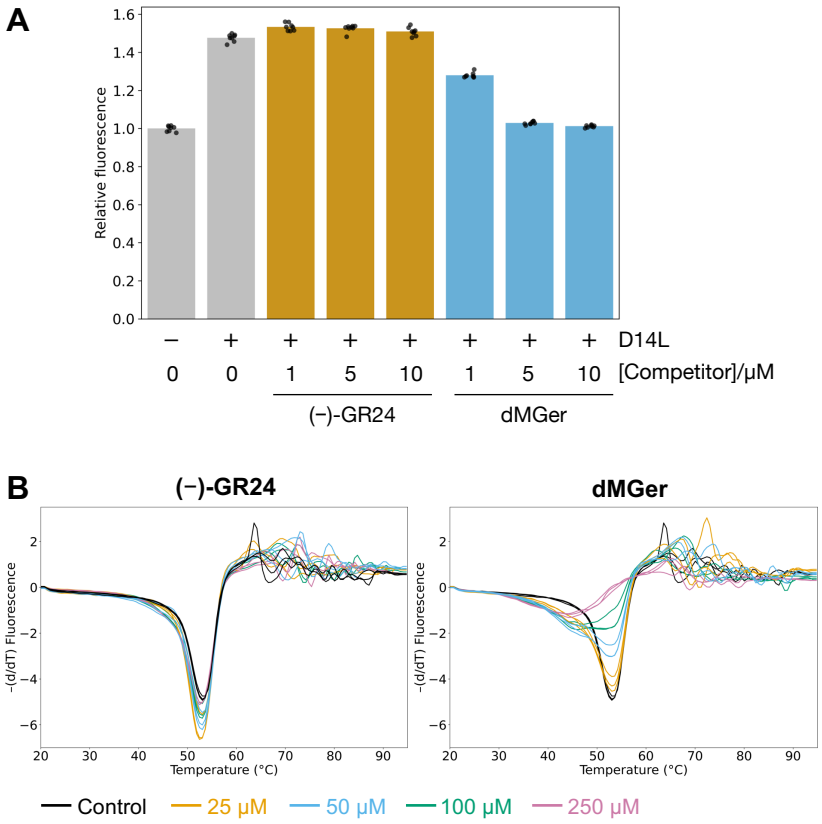

Figure 2. Binding of (−)-GR24 and desmethyl germinone to D14L *in vitro*.
(**A**) Inhibitory effects of dMGer and (−)-GR24 on dYLG hydrolysis by MBP-6×His-D14L. Reactions contained 1 μM dYLG, 10 ng/μL protein, and the indicated concentrations of (−)-GR24 or dMGer. Dimethyl sulfoxide without either compound served as the mock control. Circles represent individual data points, expressed relative to the mean fluorescence intensity of mock reactions; bars indicate means (n = 8).
(**B**) Differential scanning fluorimetry (DSF) of MBP-His-D14L in the presence of 0–100 μM (−)-GR24 (left) or desmethyl germinone (dMGer) (right). Melting curves of the protein incubated with the indicated concentrations of each compound are shown in different colors. Each line represents a single replicate (triplicates for each concentration). Control experiments, in which the protein was incubated without KL analogs, are shown in both plots.

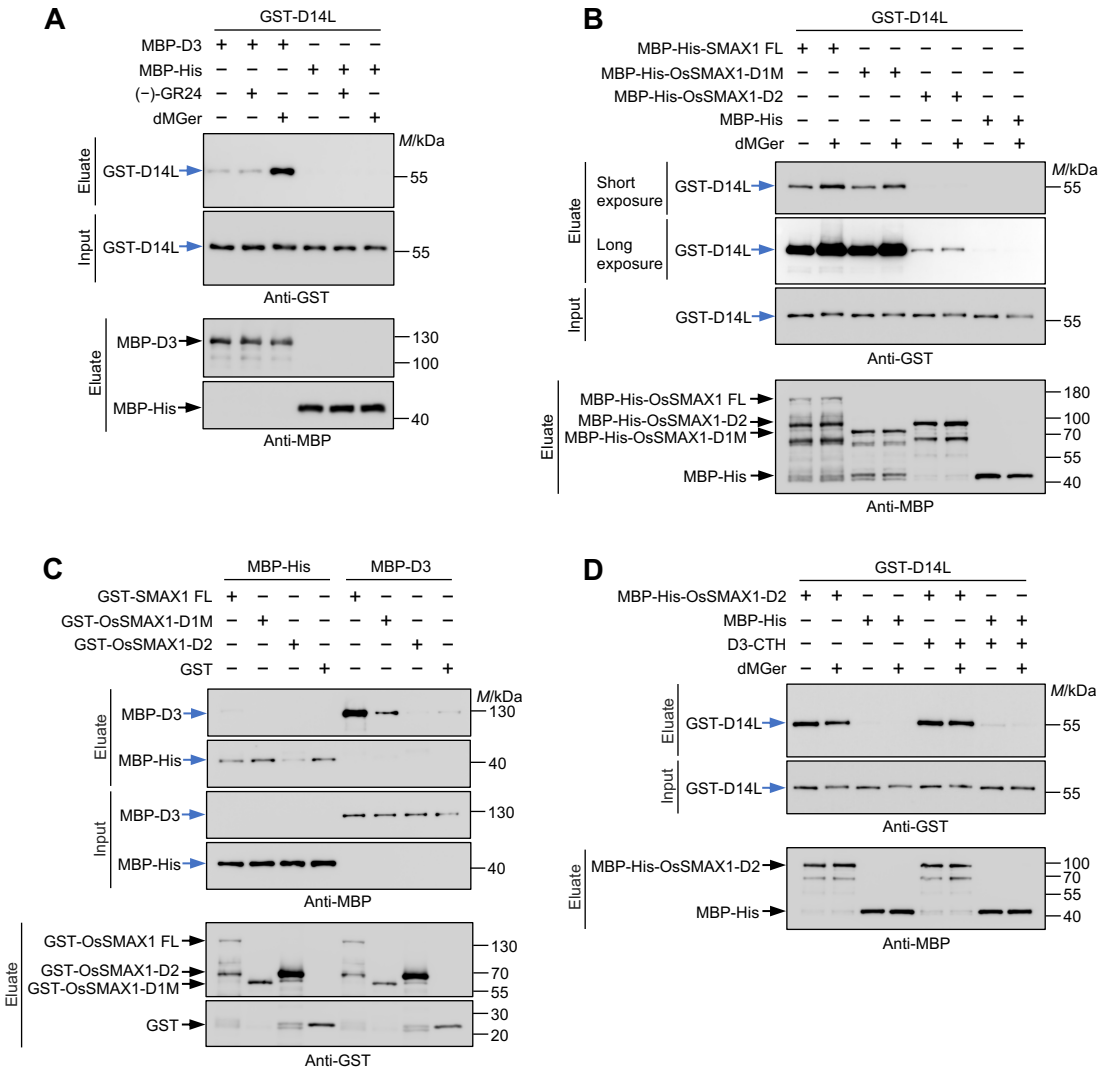

Figure 3. Interactions between KL signaling components.

(**A**) *In vitro* MBP pull-down assay using dextrin agarose beads, with MBP-D3 co-expressed with ASK1 or MBP-His tag alone as bait, and GST-D14L as prey. All reactions contained 0.2% (v/v) DMSO as solvent for chemicals. Assays were supplemented with either 10 µM dMGer, 10 µM (−)-GR24, or DMSO only. Calculated molecular masses: GST-D14L, ~56 kDa; MBP-D3, ~121 kDa; MBP-His tag, ~45 kDa.

(**B**) *In vitro* MBP pull-down assay using MBP-His-tagged full-length (FL) or domain fragments of OsSMAX1 as bait, and GST-D14L as prey. Assays were performed with or without 10 µM dMGer. For better visualization of GST-D14L pulled-down by each bait, images of the same blot taken with different exposure times (short and long) are shown. Calculated molecular masses: MBP-His-OsSMAX1 FL, ~154 kDa; MBP-His-OsSMAX1-D1M, ~79 kDa; MBP-His-OsSMAX1-D2, ~90 kDa.

(**C**) *In vitro* GST pull-down assay using glutathione agarose beads, with GST-tagged FL or domains of OsSMAX1 as bait, and MBP-D3 or MBP-His as prey. Calculated molecular masses: GST-OsSMAX1 FL, ~135 kDa; GST-OsSMAX1-D1M, ~60 kDa; GST-OsSMAX1-D2, ~71 kDa; GST tag, ~28 kDa.

(**D**) *In vitro* MBP pull-down assay using MBP-His-OsSMAX1-D2 as bait and GST-D14L as prey, performed in the presence or absence of D3-CTH peptide, with or without 10 µM dMGer.

GST- and MBP(-His)-tagged proteins were detected by immunoblotting with anti-GST and anti-MBP antibodies, respectively. The positions of size markers electrophoresed with the samples are shown alongside each blot.

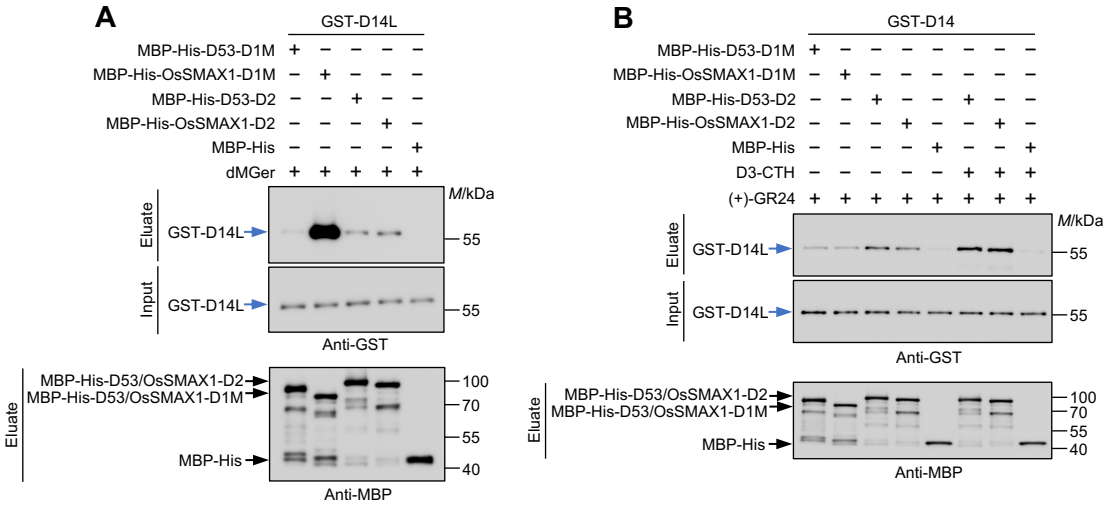

Figure 4. Differential interaction of D14L and D14 with domains of OsSMAX1 and D53.
(**A**) *In vitro* MBP pull-down assay using MBP-His-tagged domains of D53 or OsSMAX1 as bait, and GST-D14L as prey. All reactions contained 10 µM dMGer. Calculated molecular masses: MBP-His-D53-D1M, ~80 kDa; MBP-His-D53-D2, ~91 kDa.
(**B**) *In vitro* MBP pull-down assay using MBP-His-tagged domains of D53 or OsSMAX1 as bait, and GST-D14 as prey, performed in the presence or absence of D3-CTH. All reactions contained 10 µM (+)-GR24. Calculated molecular masses: GST-D14 ~56 kDa.
GST- and MBP-His-tagged proteins were detected by immunoblotting with anti-GST and anti-MBP antibodies, respectively. The positions of size markers electrophoresed with the samples are shown alongside each blot.

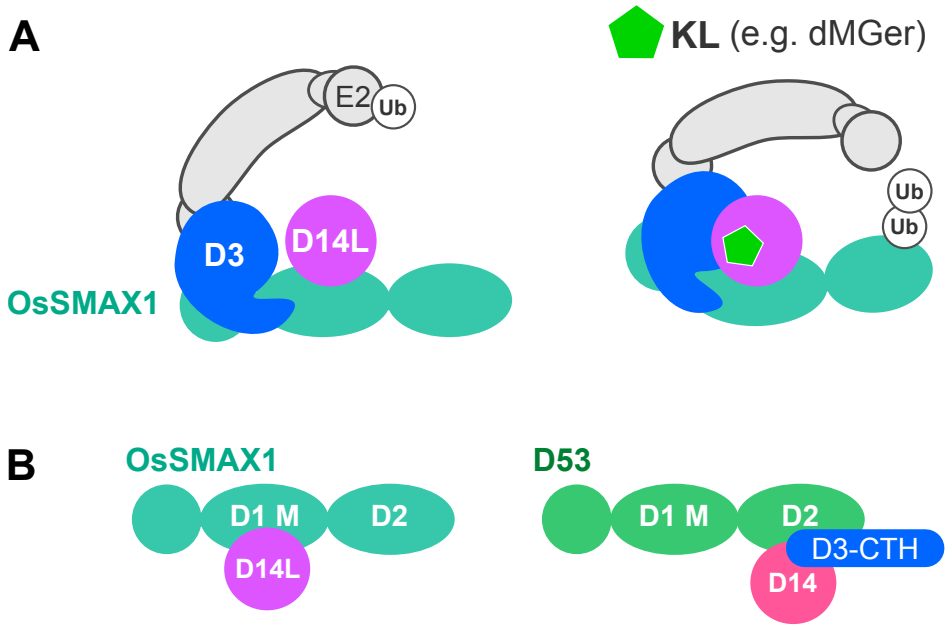

Figure 5. Interactions between rice KL signaling components and effects of KL.
(**A**) Model of KL-triggered changes in protein–protein interactions. Even in the absence of KL, OsSMAX1 interacts with both D14L and D3, potentially forming a single complex. KL promotes direct binding between D14L and D3 and enhances the interaction between D14L and OsSMAX1, likely stabilizing and altering the conformation of the complex, thereby leading to the ubiquitination of OsSMAX1. Differences in interaction strength are indicated by the thickness of grey lines.
(**B**) Schematic of physical interactions of rice D14L and D14 with domains of OsSMAX1 and D53. D14L mainly interacts with OsSMAX1-D1M, whereas D14 mainly interacts with D53-D2. D3-CTH enhances the interaction between D14 and the D53-D2 domain. Differences in interaction strength are indicated by the thickness of grey lines.